

Quasiharmonic free energy and derivatives for slabs: Oxide surfaces at elevated temperatures

M. B. Taylor, C. E. Sims, G. D. Barrera,* and N. L. Allan

School of Chemistry, University of Bristol, Cantock's Close, Bristol BS8 1TS, United Kingdom

W. C. Mackrodt

School of Chemistry, University of St. Andrews, St. Andrews, Fife KY16 9ST, Scotland

(Received 19 October 1998)

The work of Taylor *et al.* [Phys. Rev. B **56**, 14 380 (1997)], which calculates the free energy of three-dimensional periodic crystals and its analytic derivatives with respect to all the external and internal degrees of freedom using lattice statics and lattice dynamics in the quasiharmonic approximation, is extended to lattices which are periodic in only two dimensions. Derivatives are calculated by means of first-order perturbation theory and detailed expressions for all the lattice sums required are presented. The method is used to calculate the temperature variation of the surface free energy, surface structure, and density of states of some representative oxide surfaces. These include the {100} and {110} surfaces of MgO, the {100} surface of NiO, the {111} surface of Li₂O and the microfaceted {110} surface of MgO. For these systems, surface free energies decrease slightly over the range of temperatures for which the quasiharmonic approximation holds.

[S0163-1829(99)01310-7]

I. INTRODUCTION

Many technologically important areas of interest ranging from heterogeneous catalysis to high-temperature superconductivity (see, e.g., Refs. 1 and 2) utilize the properties of the surfaces of ionic oxides. In addition to experimental advances over the past decade, considerable progress has been achieved in the calculation of properties of surfaces, including surface structure, surface energy, point defect properties, and segregation characteristics.³⁻⁵ Where experimental data have been available, the agreement has been encouraging. A particularly notable example is the extensive relaxation at the {0001} basal plane of α -Al₂O₃, predicted by atomistic lattice simulations⁶ and later by first-principles density-functional theory⁷ and Hartree-Fock⁸ calculations, which has been verified substantially by recent surface x-ray measurements by Guénard *et al.*,⁹ as shown in Table I. In addition, calculated surface and/or attachment energies have been used to rationalize the crystal morphology, of, among other examples, α -Fe₂O₃,¹⁰ Fe-, Cr-, Y-, and La-doped α -Al₂O₃,⁶ BaSO₄,¹¹ SnO₂ and SrSnO₃,¹² and zircon.¹³

A potentially serious limitation of the majority of previous theoretical work on oxide surfaces is that it has been restricted to the *static* limit. Few calculations have included dynamic effects, including *temperature*, largely because the full dynamical treatment of complex solids, including crystals with large unit cells, defective crystals and surfaces, presents severe computational demands if reasonably high precision is required. For surfaces, it can be crucial, as we shall see, to take explicit account of the relaxation of a large number of layers adjacent to the surface.

There are three main simulation techniques available for the calculation of surface properties: Monte Carlo, molecular dynamics, and quasiharmonic lattice dynamics. Of these only the last is capable of giving free energies (as well as derived properties such as the entropy and the heat capacity) directly and to high precision. This method is consequently not only

the most suitable for structure optimisation as a function of temperature but in many applications it has also been shown to be a valid approximation up to two-thirds of the bulk melting temperature.^{14,15}

We have recently developed a code based on quasiharmonic lattice dynamics designed for the efficient study of three-dimensional periodic structures with *many* internal strains (degrees of freedom).¹⁶ To calculate the optimum structure of a (periodic) crystal at temperature T , and external pressure, P_{ext} , it is necessary to determine the minimum free energy with respect to all the geometrical variables that define the unit cell. Some previous approaches to this optimization (e.g., Watson *et al.*¹⁷) have used the zero static internal stress approximation (ZSISA),¹⁸ in which only the external coordinates (dimensions of the unit cell) are relaxed using fully dynamic free-energy derivatives, while internal coordinates (positions of the ions within the unit cell) are relaxed using static energy derivatives. This approach is popular since static energy derivatives can be calculated analytically, and quite rapidly, while only a small number of free-energy derivatives is required for the unit-cell dimensions and these can be readily obtained numerically. On the

TABLE I. Comparison of theoretical and experimental surface relaxations (%) of α -Al₂O₃ {0001}. $S(\text{Al})$ denotes the outer surface layer with Al atoms outermost. Inner surface layers are numbered sequentially according to increasing distance from the surface.

Layer	Mackrodt (Ref. 3)	Aprá <i>et al.</i> (Ref. 8)	Manassidis <i>et al.</i> (Ref. 7)	Guénard <i>et al.</i> (Ref. 9) (Expt.)
$S(\text{Al})$	-59	-66	-86	-51
$S-1(\text{O})$	2	1	3	16
$S-2(\text{Al})$	-49	-43	-54	-29
$S-3(\text{Al})$	26	18	25	20
$S-4(\text{O})$	8	4		

other hand, even for unit cells of moderate size, numerical differentiation of the free energy with respect to all the internal coordinates is normally prohibitively expensive. Our code SHELL (Ref. 16) for three-dimensional crystals calculates the full set of free-energy first derivatives analytically^{19,20} and a full minimization of the quasiharmonic free energy with respect to all internal and external variables for large unit cells is possible.

Here we extend this previous work to the surfaces of ionic solids by developing the theory for slablike geometries in which the crystal is finite in one direction and infinite in the other two. If the slab is sufficiently thick to provide what is effectively a bulklike region in the interior of the slab, then the two surfaces are essentially noninteracting and, in effect, are free surfaces. We give explicit expressions for the lattice sums required to calculate the slab free energy and its strain derivatives: these are the analogs of the bulk lattice sum expressions presented in Taylor *et al.*¹⁹ Thus our approach is a radical departure from the two-region strategy used by Tasker²¹ and Gay and Rohl,¹³ in which the positions (and polarizations) of the ions in the vicinity of the surface *only* are relaxed explicitly by minimizing the *internal* energy of the system, while the remainder are constrained to their bulk lattice positions. In the corresponding ZSISA approximation for slablike geometries, lattice relaxation perpendicular to the surface, which in most cases is the predominant relaxation from the bulk structure, comprises the internal strains and is thus calculated from the internal energy and not the free energy of the system. As we show later, this approximation is very poor for surfaces.

This is a report of surface free energies based on a complete minimization of the free energy. Previously, Mulheran and co-workers have used a localized Einstein-like approximation for the phonon spectrum to estimate the temperature dependence of surface energies.^{22–24} Molecular-dynamics simulations have been used to study the {001} surface of KCl (Ref. 25) and NiO.²⁶ Here we report calculations for the {001} and {110} surfaces of MgO, for the {001} surface of NiO (for comparison with Mulheran²⁴), and the {111} surface of Li₂O. The {001} and {110} surfaces of MgO and NiO are type I, according to the Tasker classification;²⁷ the surface layers are neutral and contain all component ions in their stoichiometric ratio. The {111} surface of Li₂O is type II,²⁷ since the surface is comprised of only one type of ion even though there is no dipole moment perpendicular to the surface. We have also evaluated the temperature dependence of the microfaceted {110} surface of MgO, which, in the static limit, has been studied by Watson *et al.*²⁸

At present our approach to temperature effects can use two and three-body potentials, and the calculations reported here are all based on simple two-body potentials. As Table I illustrates for α -Al₂O₃, there is remarkably good agreement between results, subsequently confirmed by experiment, obtained using two-body potentials and those from *ab initio* calculations in the static limit; this suggests that potentials of this type can be used to describe dynamics properties of the kind reported here.

II. THEORY

A. Slab structure and strain coordinates

Slab structures can be defined in terms of two lattice vectors \mathbf{a}_1 and \mathbf{a}_2 . The corresponding reciprocal lattice vectors, \mathbf{b}_1 and \mathbf{b}_2 , are given by

$$\mathbf{b}_1 = \frac{2\pi}{A^2} \mathbf{a}_2 \times (\mathbf{a}_1 \times \mathbf{a}_2), \quad (1)$$

$$\mathbf{b}_2 = \frac{2\pi}{A^2} \mathbf{a}_1 \times (\mathbf{a}_2 \times \mathbf{a}_1), \quad (2)$$

where A is the area of the unit cell ($=|\mathbf{a}_1 \times \mathbf{a}_2|$).

Much of the development of this section derives from that in Taylor *et al.*,¹⁹ the equations of which are referred to as (Tn). The particles which comprise the slab, which in a shell model²⁹ may be cores or shells, have Cartesian coordinates, r_{ix}^α , given by

$$r_{ix}^\alpha = \sum_{\gamma} (\delta_{\alpha\gamma} + e^{\alpha\gamma})(x^\gamma + \rho_i^\gamma), \quad (3)$$

where Greek subscripts and superscripts are indices x, y or z labeling Cartesian axes oriented such that the surface lattice vectors lie in the xy plane.³⁰ \mathbf{x} is a surface lattice vector, $i = 1, \dots, n$ is an index that labels a specific particle within a unit cell, and $\delta_{\alpha\beta}$ is the Kronecker delta. Components of the tensor $e^{\alpha\beta}$ determine both the orientation and the macroscopic state of the strain. The vector components ρ_i^γ are internal coordinates determining the positions of particles within a unit cell of the slab. Since we work always at constant surface area we need only derivatives of the free energy with respect to the ρ_i^γ (cf. Taylor *et al.*¹⁹ where, for the three-dimensional case, derivatives with respect to the $e^{\alpha\beta}$ are given). In some applications symmetry reduces the number of independent coordinates and it is possible to define a set of ‘‘symmetric internal coordinates’’ w_m [Eq. (T4)] that allow a description of the structure with a reduced number of variables. In general, the geometry can be characterized by, and the free energy differentiated with respect to an $N_{\mathcal{E}}$ -element vector of generalized coordinates \mathcal{E}_A . Here the \mathcal{E}_A may comprise the ρ_i^γ or the w_m .

In order to optimize the structure of the slab, i.e., to find the most stable state under a given set of thermodynamic constraints, it is necessary to minimize the appropriate thermodynamic potential with respect to the $N_{\mathcal{E}}$ structure parameters \mathcal{E}_A . Since we are here interested solely in surfaces at zero pressure, the appropriate potential is the Helmholtz energy F .

B. Free-energy evaluation and strain derivatives

In the quasiharmonic approximation it is assumed that the Helmholtz energy at temperature T can be written as the sum of static and vibrational contributions,

$$F(\mathcal{E}, T) = \Phi_{\text{stat}}(\mathcal{E}) + F_{\text{vib}}(\mathcal{E}, T). \quad (4)$$

Φ_{stat} is the potential energy of the static lattice in a given state of strain \mathcal{E} , and F_{vib} is the sum of harmonic vibrational contributions from all the normal modes. For a periodic structure, the frequencies $\nu_j(\mathbf{q})$ of modes with wave vector \mathbf{q} are obtained by diagonalization of the dynamical matrix $D(\mathbf{q})$ in the usual way (e.g., Wallace³²). F_{vib} is given by

$$F_{\text{vib}} = \sum_{\mathbf{q},j} \left\{ \frac{1}{2} h \nu_j(\mathbf{q}) + k_B T \ln [1 - \exp(-h \nu_j(\mathbf{q})/k_B T)] \right\}, \quad (5)$$

and the associated vibrational entropy, S , and internal energy U_{vib} by

$$S = \sum_{\mathbf{q},j} \left\{ \frac{(h \nu_j(\mathbf{q})/T)}{\exp(h \nu_j(\mathbf{q})/k_B T) - 1} - k \ln [1 - \exp(-h \nu_j(\mathbf{q})/k_B T)] \right\} \quad (6)$$

$$U_{\text{vib}} = \sum_{\mathbf{q},j} \left\{ \frac{1}{2} h \nu_j(\mathbf{q}) + \frac{h \nu_j(\mathbf{q})}{\exp(h \nu_j(\mathbf{q})/k_B T) - 1} \right\}, \quad (7)$$

in which the first term in the expressions for F_{vib} and U_{vib} is the zero-point energy. For a macroscopic crystal the sum over \mathbf{q} becomes an integral over a cell in reciprocal space, which can be evaluated by taking successively finer uniform grids until convergence is achieved. Since the reciprocal space is now two-dimensional the Brillouin zone requires a two-dimensional mesh of wave vectors—it is straightforward to implement the two-dimensional analog³¹ of one of the usual meshes.

There are now two ways to continue. The minimization of F and subsequent thermodynamic manipulation can of course be carried out by brute force, from numerical values of F obtained using Eq. (5). However, for the type of surfaces we wish to examine here and elsewhere, the corresponding slabs are characterized by large numbers of internal strains so that it is much more efficient to use analytic expressions for the derivatives of F with respect to strain. The strain derivatives are given by

$$\left(\frac{\partial F_{\text{vib}}}{\partial \mathcal{E}_A} \right)_{\mathcal{E}', T} = \sum_{\mathbf{q},j} \left\{ \frac{h}{2 \nu_j(\mathbf{q})} \left(\frac{1}{2} + \frac{1}{\exp(h \nu_j(\mathbf{q})/k_B T) - 1} \right) \times \left(\frac{\partial \nu_j^2(\mathbf{q})}{\partial \mathcal{E}_A} \right)_{\mathcal{E}'} \right\}, \quad (8)$$

where the subscript \mathcal{E}' denotes that all the \mathcal{E} are kept constant except for the differentiation variable. We thus require derivatives of the frequencies. In our code¹⁶ the derivatives $[\partial \nu_j^2(\mathbf{q})/\partial \mathcal{E}_A]_{\mathcal{E}'}$ are obtained from the analytic expressions for the derivatives $[\partial D(\mathbf{q})/\partial \mathcal{E}_A]_{\mathcal{E}'}$ by first-order perturbation theory.^{19,32} A crucial point here is that for obtaining derivatives the perturbation is infinitesimal and the procedure exact. In addition, for thermodynamic properties no special consideration needs to be given to degeneracies in first-order perturbation theory, since the trace of $[\partial D(\mathbf{q})/\partial \mathcal{E}_A]_{\mathcal{E}'}$ is invariant for any complete normal set of eigenvectors of D .

To obtain the equilibrium structure a variable metric method³³ is used to minimize F with respect to the \mathcal{E}_A . In the initial configuration the *static* energy Hessian, $(\partial^2 \Phi_{\text{stat}}/\partial \mathcal{E}_A \partial \mathcal{E}_B)$, which is a good approximation to $(\partial^2 F/\partial \mathcal{E}_A \partial \mathcal{E}_B)$, is calculated from its analytic expression, and its inverse together with the $(\partial F/\partial \mathcal{E}_A)$ is used to obtain an improved configuration. In subsequent iterations the $(\partial F/\partial \mathcal{E}_A)$ are calculated in the configurations and the inverse Hessian updated by the Broden-Fletcher-Goldfarb-Shanno

formula.³⁴ An optimization therefore requires one static Hessian calculation, and a small number of dynamic gradient calculations. We have found this to be much more efficient than methods involving repeated evaluation of the Hessian, or frequent line minimizations or in which the derivatives are determined numerically. For more details, discussion of scaling aspects and examples, see Ref. 16.

C. Lattice sums for short-range potentials

The same approach may be followed as in the three-dimensional analog with no special treatment for slab geometries. The expressions required for general short-range two and three-body potentials are given by Taylor *et al.*^{19,20}

D. Lattice sums for Coulomb interactions

The two-dimensional Ewald summation has a different form from that in three-dimensions. We start from the result³⁵⁻³⁷ for a slab periodic in two-dimensions but aperiodic in the third:

$$\sum_{\mathbf{x}} \frac{e^{i\mathbf{q} \cdot \mathbf{x}}}{r_{\mathbf{x}}} (1 - \delta'_{ij\mathbf{x}}) = \sum_{\mathbf{x}} e^{i\mathbf{q} \cdot \mathbf{x}} X^0(r_{\mathbf{x}}) + \sum_{\mathbf{k}}' e^{-i\mathbf{q}_{\mathbf{k}} \cdot \mathbf{r}} Q(q_{\mathbf{k}}, r^z) - \delta_{q_0} R(r^z), \quad (9)$$

where

$$R(r^z) = \frac{2\pi}{A} \left[\frac{1}{\eta \sqrt{\pi}} \exp(-(\eta r^z)^2) + r^z \operatorname{erf}(\eta r^z) \right], \quad (10)$$

$$Q(k, r^z) = \frac{\pi}{Ak} \left[\exp(kr^z) \operatorname{erfc}\left(\frac{k}{2\eta} + \eta r^z\right) + \exp(-kr^z) \operatorname{erfc}\left(\frac{k}{2\eta} - \eta r^z\right) \right]. \quad (11)$$

Equation (11) may be compared with its three-dimensional equivalent (T101). The two share the same notation. $\delta'_{ij\mathbf{x}}$ is zero unless either (a) $\mathbf{x}=0$ and $i=j$ or (b) $\mathbf{x}=0$ and i and j are shell and core of the same ion. In a rigid-ion system, only case (a) arises. The factor $(1 - \delta'_{ij\mathbf{x}})$ therefore properly eliminates the Coulombic interaction of an ion with itself. The \mathbf{x} summation is over all surface lattice vectors and the \mathbf{k} summation over all reciprocal-lattice vectors omitting $\mathbf{q}=\mathbf{k}=0$ (as indicated by the prime). η is an arbitrary parameter, which can be chosen so that good accuracy is achieved when both sums are truncated after a small number of terms going out from their respective origins. $\eta = \sqrt{\pi} A^{-1/2}$ is a reasonable choice. Additional quantities, also used in Ref. 19 are

$$\mathbf{r} = \mathbf{r}_{ij}, \quad (12)$$

$$\mathbf{r}_{\mathbf{x}} = \mathbf{r} + \mathbf{x}, \quad (13)$$

$$\mathbf{q}_{\mathbf{k}} = \mathbf{q} + \mathbf{k}, \quad (14)$$

$$\delta_{q_0} = \begin{cases} 1, & \mathbf{q} = 0 \\ 0, & \text{otherwise,} \end{cases} \quad (15)$$

$$X^0(r_{\mathbf{x}}) = \frac{\operatorname{erfc}(\eta r_{\mathbf{x}}) - \delta'_{ij\mathbf{x}}}{r_{\mathbf{x}}}. \quad (16)$$

The same approach can then be used as in Ref. 19. It is possible [Eqs. (T70)–(T78)] to construct the energy, dynamical matrix and the required internal coordinate derivatives in terms of two sets of matrices, \mathbf{S} and \mathbf{T} :

$$\Phi_{\text{stat}} = \frac{1}{2} \sum_{ij} S_{ij}, \quad (17)$$

$$\left(\frac{\partial \Phi_{\text{stat}}}{\partial \rho_k^\alpha} \right) = \sum_i (1 - \delta_{ik}) S_{ik}^\alpha, \quad (18)$$

$$\left(\frac{\partial^2 \Phi_{\text{stat}}}{\partial \rho_k^\alpha \partial \rho_l^\beta} \right) = \delta_{kl} \sum_i (1 - \delta_{ik}) S_{ik}^{\alpha\beta} - (1 - \delta_{kl}) S_{kl}^{\alpha\beta}, \quad (19)$$

$$B_{ij}^{\alpha\beta}(\mathbf{q}) = \delta_{ij} \sum_k T_{ik}^{\alpha\beta}(0) - T_{ij}^{\alpha\beta}(\mathbf{q}), \quad (20)$$

$$\begin{aligned} \left(\frac{\partial B_{ij}^{\alpha\beta}(\mathbf{q})}{\partial \rho_k^\gamma} \right) &= \delta_{ik} \delta_{jk} \sum_l T_{lk}^{\alpha\beta\gamma}(0) + \delta_{ij} T_{ik}^{\alpha\beta\gamma}(0) \\ &+ (\delta_{ik} - \delta_{jk}) T_{ij}^{\alpha\beta\gamma}(\mathbf{q}). \end{aligned} \quad (21)$$

The elements of the dynamical matrix $D_{ij}^{\alpha\beta}(\mathbf{q})$ and its derivatives are related to $B_{ij}^{\alpha\beta}(\mathbf{q})$ via (T18) and (T34). Derivatives with respect to the symmetric internal coordinates w_m rather than the ρ_i can be obtained using Eq. (T4).

Since the real-space part of the slab expression [Eq. (9)] is the same as that for the three-dimensional equivalent [Eq. (T101)], the real-space part of all the derivatives will not change from the three-dimensional case [Eqs. (T111), (T112), (T114), (T117), (T118)]. We concern ourselves here therefore only with the reciprocal space parts.

We define a set of functions

$$R^{*\alpha}(r^z) = \frac{\partial}{\partial r^\alpha} R^*(r^z), \quad (22)$$

$$Q^{*\alpha}(k, r^z) = \frac{\partial}{\partial r^\alpha} Q^*(k, r^z), \quad (23)$$

where in these equations the superscript (*) indicates any sequence of zero or more indices x, y, z (Greek letter superscripts). Then the reciprocal space parts of the relevant expressions for slab geometry can be written

$$\frac{S_{ij[\text{recip}]}}{Z_{ij}} = \sum_{\mathbf{k}}' \cos(\mathbf{k} \cdot \mathbf{r}) Q(k, r^z) - R(r^z), \quad (24)$$

$$\begin{aligned} \frac{S_{ij[\text{recip}]}}{Z_{ij}} &= \sum_{\mathbf{k}}' [\cos(\mathbf{k} \cdot \mathbf{r}) Q^\alpha(k, r^z) - \sin(\mathbf{k} \cdot \mathbf{r}) k^\alpha Q(k, r^z)] \\ &- R^\alpha(r^z), \end{aligned} \quad (25)$$

$$\begin{aligned} \frac{S_{ij[\text{recip}]}}{Z_{ij}} &= \sum_{\mathbf{k}}' \{ \cos(\mathbf{k} \cdot \mathbf{r}) [Q^{\alpha\beta}(k, r^z) - k^\alpha k^\beta Q(k, r^z)] \\ &- \sin(\mathbf{k} \cdot \mathbf{r}) [k^\alpha Q^\beta(k, r^z) + k^\beta Q^\alpha(k, r^z)] \} \\ &- R^{\alpha\beta}(r^z), \end{aligned} \quad (26)$$

$$\begin{aligned} \frac{T_{ij[\text{recip}]}^{\alpha\beta}(\mathbf{q})}{Z_{ij}} &= \sum_{\mathbf{k}}' e^{-i\mathbf{q}_k \cdot \mathbf{r}} [Q^{\alpha\beta}(q_{\mathbf{k}}, r^z) - q_{\mathbf{k}}^\alpha q_{\mathbf{k}}^\beta Q(q_{\mathbf{k}}, r^z) \\ &- i q_{\mathbf{k}}^\alpha Q^\beta(q_{\mathbf{k}}, r^z) - i q_{\mathbf{k}}^\beta Q^\alpha(q_{\mathbf{k}}, r^z)] \\ &- \delta_{q_0} R^{\alpha\beta}(r^z), \end{aligned} \quad (27)$$

$$\begin{aligned} \frac{T_{ij[\text{recip}]}^{\alpha\beta\gamma}(\mathbf{q})}{Z_{ij}} &= \sum_{\mathbf{k}}' e^{-i\mathbf{q}_k \cdot \mathbf{r}} [Q^{\alpha\beta\gamma}(q_{\mathbf{k}}, r^z) - q_{\mathbf{k}}^\beta q_{\mathbf{k}}^\gamma Q^\alpha(q_{\mathbf{k}}, r^z) \\ &- q_{\mathbf{k}}^\alpha q_{\mathbf{k}}^\gamma Q^\beta(q_{\mathbf{k}}, r^z) - q_{\mathbf{k}}^\alpha q_{\mathbf{k}}^\beta Q^\gamma(q_{\mathbf{k}}, r^z) \\ &- i q_{\mathbf{k}}^\alpha Q^\beta Q^\gamma(q_{\mathbf{k}}, r^z) - i q_{\mathbf{k}}^\beta Q^\alpha Q^\gamma(q_{\mathbf{k}}, r^z) \\ &- i q_{\mathbf{k}}^\gamma Q^\alpha Q^\beta(q_{\mathbf{k}}, r^z) + i q_{\mathbf{k}}^\alpha q_{\mathbf{k}}^\beta q_{\mathbf{k}}^\gamma Q(q_{\mathbf{k}}, r^z)] \\ &- \delta_{q_0} R^{\alpha\beta\gamma}(r^z), \end{aligned} \quad (28)$$

where Z_{ij} is the Coulomb factor

$$Z_{ij} = \frac{z_i z_j}{4\pi\epsilon_0}, \quad (29)$$

and z_i is the charge on particle i . The forms of the $R^*(r^z)$ and $Q^*(k, r^z)$ functions are determined by repeated application of Eqs. (22) and (23) to Eqs. (10) and (11). By observation, if any of the indices α represented by the superscript (*) is not equal to z , then the corresponding function will be zero.

The nonzero R functions are given by

$$R^z(r^z) = \frac{2\pi}{A} \text{erf}(\eta r^z), \quad (30)$$

$$R^{zz}(r^z) = \frac{4\sqrt{\pi}\eta}{A} \exp(-(\eta r^z)^2), \quad (31)$$

$$R^{zzz}(r^z) = \frac{-8\sqrt{\pi}\eta^3}{A} \exp(-(\eta r^z)^2). \quad (32)$$

The Q functions are somewhat more lengthy and most easily expressed in terms of intermediate functions. Defining

$$F(k, r^z) = \exp(k r^z) \text{erfc}\left(\frac{k}{2\eta} + \eta r^z\right), \quad (33)$$

$$E(k, r^z) = \pi^{-1/2} \exp\left[-\left(\frac{k}{2\eta}\right)^2 - (\eta r^z)^2\right], \quad (34)$$

$$P(k, r^z) = \frac{\pi}{A} [F(k, r^z) + F(k, -r^z)], \quad (35)$$

$$M(k, r^z) = \frac{\pi}{A} [F(k, r^z) - F(k, -r^z)], \quad (36)$$

$$G(k, r^z) = \frac{\pi}{A} [E(k, r^z) + E(k, -r^z)] = \frac{2\pi}{A} E(k, r^z), \quad (37)$$

which lead to the relations

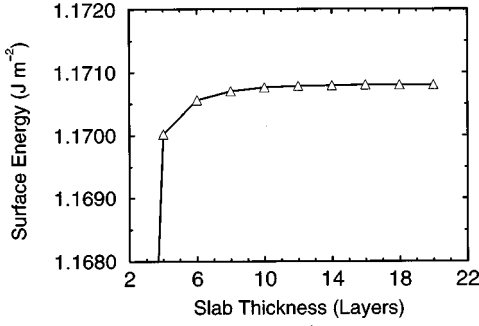


FIG. 1. Variation of the MgO {100} surface free energy with slab thickness.

$$\frac{\partial}{\partial r^z} P(k, r^z) = kM(k, r^z), \quad (38)$$

$$\frac{\partial}{\partial r^z} M(k, r^z) = kP(k, r^z) - 2\eta G(k, r^z), \quad (39)$$

$$\frac{\partial}{\partial r^z} G(k, r^z) = -2\eta^2 r^z G(k, r^z). \quad (40)$$

It is then straightforward to derive the following expressions for the nonzero Q functions:

$$Q(k, r^z) = P(k, r^z)k^{-1}, \quad (41)$$

$$Q^z(k, r^z) = M(k, r^z), \quad (42)$$

$$Q^{zz}(k, r^z) = P(k, r^z)k - G(k, r^z)2\eta, \quad (43)$$

$$Q^{zzz}(k, r^z) = M(k, r^z)k^2 + G(k, r^z)4\eta^3 r^z. \quad (44)$$

In calculating lattice sums for large numbers of atoms, both computational efficiency and economy of storage must be considered. With our approach it is not necessary to store the whole set of derivatives of the dynamical matrix simultaneously. Instead, the matrices \mathbf{S} and \mathbf{T} are calculated once for each wave vector and the required derivatives constructed from these and used one at a time.

III. SURFACE FREE ENERGIES

A. MgO

We start with the {100} and {110} surfaces of MgO (both Type I) and use the interatomic potentials of Stoneham and Sangster.³⁸ Irregularities such as ledges, kinks, steps, and electronic defects, present on real surfaces, are ignored. Figure 1 shows the dynamically relaxed {100} surface free energy as a function of slab thickness, which indicates that approximately ten layers are required for convergence to 0.001 J m^{-2} . This is more than twice the number of layers (4) required to converge the static energy. Figure 2 shows the calculated temperature dependence of the {100} and {110} surface free energies, based on slabs containing 12 layers. The inclusion of the zero-point energy contribution reduces the surface energy at 0 K, from 1.180 to 1.179 J m^{-2} . The {100} surface energy decreases slightly with temperature (Fig. 2), less markedly than as predicted for the {100} surface of NiO by Mulheran.²⁴

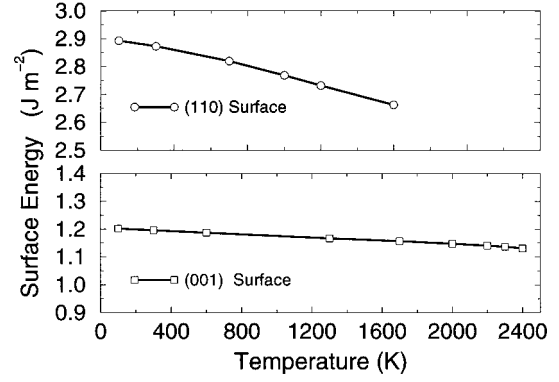


FIG. 2. Calculated temperature variation of the free energy of the {100} and {110} surfaces of MgO.

The importance of using a sufficient number of \mathbf{q} vectors to achieve convergence is illustrated by the plots in Fig. 3. Too small a number of \mathbf{q} vectors leads in general to a much smaller decrease of surface free energy with temperature than is shown by the converged values. We find it is crucial to take adequate account of long-wavelength modes by using a grid of sufficient size in the reciprocal-space summation. Equivalently, as indicated by preliminary calculations,³⁹ in any molecular-dynamics simulation the cell size must be sufficient to permit such motions. Similarly, Oliver *et al.*²⁶ suggest the {100} surface energy of NiO increases with temperature from 0 K to the melting point, which is not in agreement with our results, and is likely to be an artifact due to the small number of atoms used in their molecular-dynamics calculations.

In contrast to the {100} surface at 0 K, the inclusion of the zero-point contribution increases the {110} surface energy from a static value of 1.18 to 1.20 J m^{-2} . The {110} surface also shows a rather more marked decrease with temperature than the {001} surface, as is clear from Fig. 2. For this surface, the quasiharmonic approximation breaks down at $\approx 1600 \text{ K}$ with the appearance of imaginary frequencies. The corresponding temperatures at which imaginary frequencies appear for the bulk and the {001} surface are ≈ 2900 and $\approx 2600 \text{ K}$, respectively, which indicates that the quasiharmonic approximation fails at somewhat lower temperatures for the surfaces than for the bulk due to the presence of some

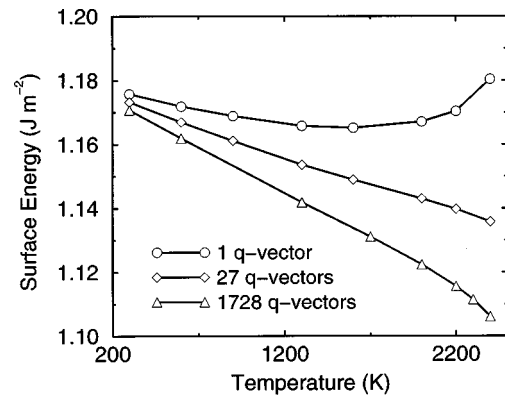


FIG. 3. Variation of the MgO {100} surface free energy with number of \mathbf{q} vectors used in the reciprocal sum summations.

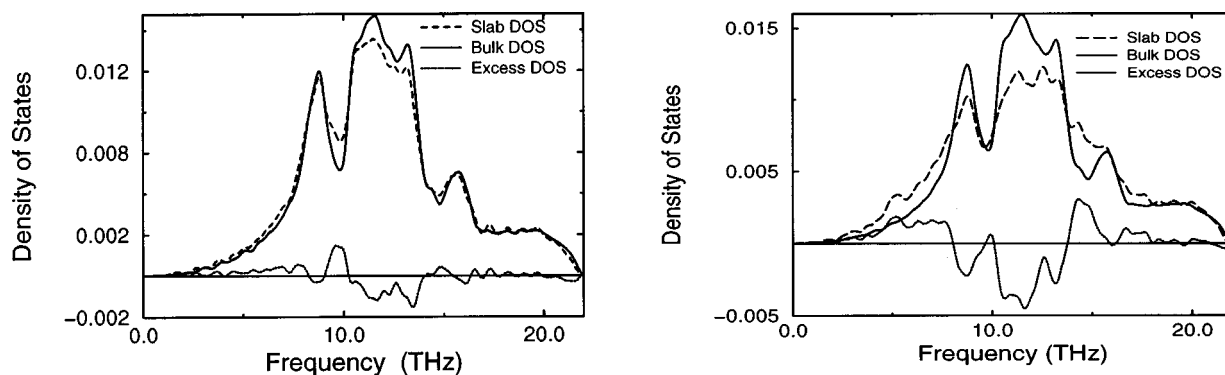


FIG. 4. Calculated bulk, surface and excess (surface minus bulk) densities of states at 700 K for the $\{100\}$ and $\{110\}$ surfaces of MgO.

modes with large amplitudes of vibration. It is tempting to suggest from this that surface melting occurs at temperatures below that of the bulk, which for MgO is ≈ 3100 K. Bulk and surface vibrational density of states (DOS) at 700 K for both $\{100\}$ and $\{110\}$ surfaces are shown in Fig. 4, the surface plots show a generalized Rayleigh mode at frequencies < 5 THz. Also plotted in Fig. 4 are the excess DOS (surface minus bulk) which is responsible for the dynamic contribution to the surface free energies. For both surfaces these show decreases in intensity of bulk modes in the range 10–14 THz. There are several surface-localized modes. Up to ≈ 18 THz the excess DOS for the $\{100\}$ surface is in good agreement with the experimental measurements of Rieder⁴⁰ close to 800 K. The calculated excess DOS does not show the peak reported above 18 THz. Our calculations do not support an earlier suggestion⁴¹ that surface relaxation at elevated temperature is responsible for this feature.

Figure 5 shows the temperature variation of the various entropic, vibrational, and internal energy contributions to the dynamically relaxed $\{100\}$ surface free energy. First, note that the vibrational internal energy and zero-point contributions are both very small and nearly equal. At high temperatures, in the classical limit, the vibrational internal energy contributes equally to both slab and bulk so that the net effect on the surface free energy is zero. As for the zero-point energy, each vibrational mode contributes $(h\nu/2)$ and so *all* frequencies contribute to the small negative difference in zero-point energy between surface and bulk. At low temperatures, only low-frequency modes are thermally excited

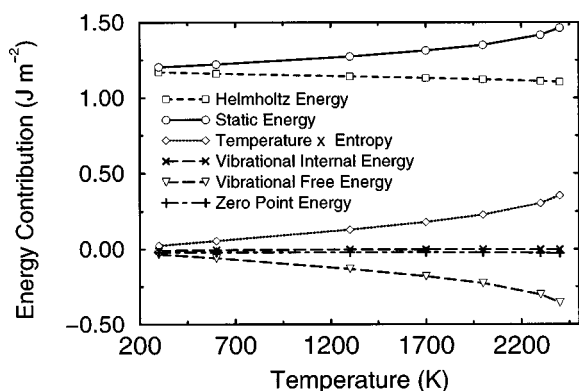


FIG. 5. Temperature variation of the surface entropy and internal energy contributions to the $\{100\}$ surface free energy of MgO.

so contributing to the entropy and hence the thermal expansion; the excess (surface minus bulk) entropy is positive. At nonzero temperatures, the entropy term, $-TS$, dominates the excess static energy and total internal energy both of which increase with temperature, unlike the surface free energy. For all the surfaces studied here, the coordination numbers of the surface ions, though smaller than in the bulk, are still relatively high, so that the (positive) expansion of the surface interlayer spacing is governed, as is that of the bulk, by the “bond-stretching” effect,⁴² in which the asymmetry of the form of the interionic potential leads to an increase of the mean interatomic distance with increasing amplitude of vibrations. It will be particularly interesting in future work to study surfaces where the structure is more open and the coordination numbers much lower. In such cases where the vibration includes components of perpendicular motion relative to a bond, a “tension effect”⁴² may dominate, leading to a thermal contraction of the surface layers.

We have also studied one example of nonplanar surfaces—the $(a/\sqrt{2})/2$ and $a\sqrt{2}$ microfaceted $\{110\}$ sur-

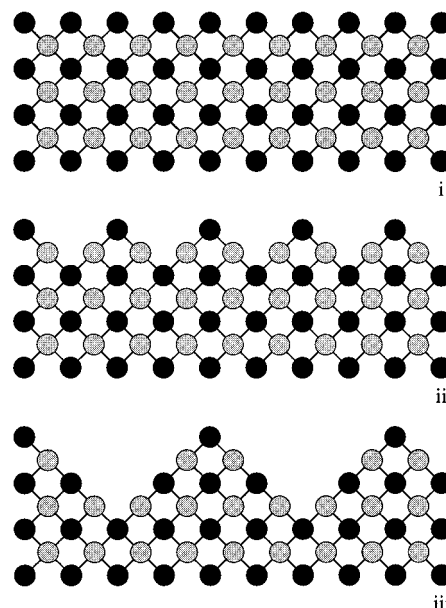


FIG. 6. (i) Unfaceted, (ii) $(a/\sqrt{2})/2$ faceted, and (iii) $a\sqrt{2}$ microfaceted $\{110\}$ surfaces of MgO. Black circles are magnesium; gray, oxide ions.

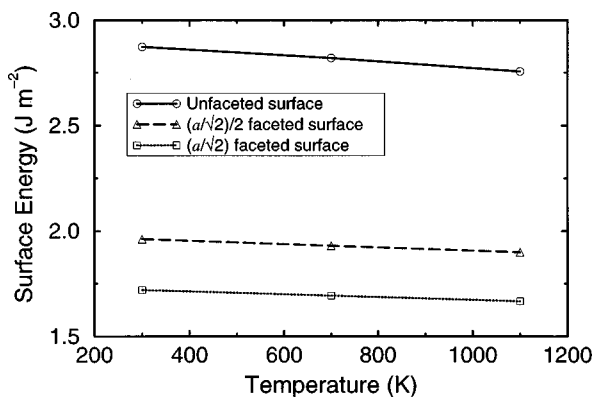


FIG. 7. Temperature variation of the surface energies of the (i) unfaceted, (ii) $(a/\sqrt{2})/2$ faceted, and (iii) $a\sqrt{2}$ microfaceted $\{110\}$ surfaces of MgO.

faces of MgO, in which rows of cations and anions are removed from the unfaceted surface as shown in Fig. 6. Surfaces of this type have been observed experimentally using low-energy electron diffraction (LEED) and scanning electron microscopy.⁴³ An alternative description of these structures is as a set of stepped $\{100\}$ surfaces. Figure 7 shows that the temperature variation of the surface free energies is indeed intermediate between those noted earlier for the planar $\{100\}$ and $\{110\}$ surfaces. It is clear that as the faceting gets more extensive, more $\{100\}$ surface is generated, with a consequent lowering of the surface energy and reduced temperature variation, which reflects the differences between the $\{100\}$ and $\{110\}$ surfaces. Thus our calculations suggest that for relatively simple faceting of this type the introduction of steps at the surface does not appear to lead to features other than those associated with the parent surfaces. One possible explanation for the peak at high frequencies seen in the experimental excess DOS (Ref. 40) for the $\{100\}$ surface is thus the presence of steps on the surface.

B. NiO

Here we consider the $\{001\}$ surface (type I) of NiO for direct comparison with the results of Mulheran²⁴ obtained using an Einstein approximation. Irregularities such as ledges, kinks, steps, and electronic defects, present on real

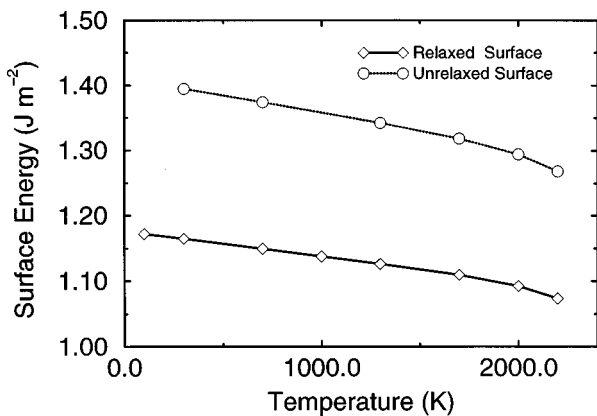


FIG. 8. Calculated temperature variation of the dynamically relaxed and unrelaxed free energy of the $\{001\}$ surface of NiO.

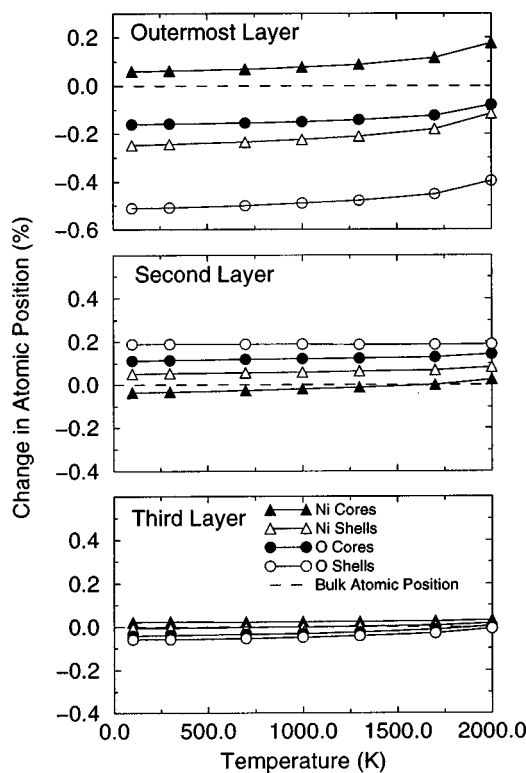


FIG. 9. Calculated temperature variation of the positions of the surface ions relative to bulk (expressed as the percentage shift in atomic position from that of the bulk) in the outer three layers for the $\{001\}$ surface of NiO, approximated by a slab of 12 layers.

surfaces, are ignored. Like Mulheran²⁴ we use the well-established set of interionic potentials due to Stoneham and Sangster.⁴⁴ Figure 8 shows the calculated temperature dependence of the unrelaxed and the fully dynamically relaxed $\{001\}$ surface energy of NiO. We find that, for the relaxed surface, at temperatures up to 2500 K 12 layers are sufficient for convergence in the surface energy to 0.0003 J m^{-2} ; a smaller number of layers is required for comparable convergence in the unrelaxed energy. The number of layers for convergence in the static limit is smaller still. At 0 K the fully relaxed dynamic surface energy is 1.19 J m^{-2} which compares with a value of $\approx 1.15 \text{ J m}^{-2}$ calculated by Mulheran.²⁴ Our value of the surface energy in the static limit, 1.18 J m^{-2} , also compares favorably with that of 1.23 J m^{-2} from *ab initio* Hartree-Fock calculations.⁴⁵ Unlike MgO $\{100\}$ inclusion of the zero-point energy thus increases the surface energy slightly. As shown in Fig. 8, both the relaxed and unrelaxed $\{001\}$ surface energies decrease slightly by $\approx 0.1 \text{ J m}^{-2}$ over the temperature range 0–2000 K, the unrelaxed surface shows a similar variation. The change of the dynamically relaxed surface energy with temperature over this range is approximately one-third of that reported by Mulheran²⁴ for the same surface, which gives an indication of the limitations of the Einstein approximation. There is no direct experimental data for comparison, but the temperature variation is at least consistent with that noted for rocksalt (001) surfaces by Benson and Yun.⁴⁶

The positions of the Ni and O ions (cores and shells) in the outermost three layers of a slab containing 12 layers are plotted as a function of temperature in Fig. 9, where all the

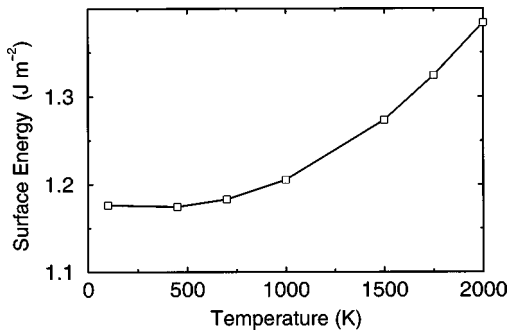


FIG. 10. Calculated temperature variation of the free energy of the {100} surface of NiO, using the ZSISA approximation as described in the text.

positions are relative to that of the middle layer of the slab. The relaxations, which for the two outermost layers result in a decrease in separation from that in the bulk of 0.3%, are qualitatively similar to those noted by Mulheran.²⁴ However the temperature variation of the positions of the ions, as with the surface free energies, is smaller than those obtained with the Einstein approximation. The qualitative features of the 0 K surface dilation, which, as expected, decreases away from the surface, are retained at elevated temperature. The rumpling of the second and third layers decreases with temperature. Once again there is good agreement with first-principles Hartree-Fock calculations⁴⁵ which have found a contraction of the first interlayer spacing of 0.53%, which supports further our use of two-body potentials in free-energy calculations for ionic systems. Furthermore, we note that the collection of reported theoretical relaxations, both here and elsewhere, are all well within an *upper bound* of $\sim 2\%$ suggested from LEED studies,⁴⁷ which attests to the increasing reliability of theoretical methods in the surface science of ionic oxides.

We now compare our results with those obtained using ZSISA. For application to surfaces where the surface lattice vectors are fixed by the lattice parameters of the corresponding bulk material, ZSISA requires a minimum of the static energy with respect to each internal strain with the other strains and the cell area, A held constant, i.e.,

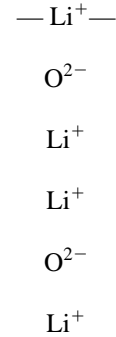
$$\left(\frac{\partial \Phi_{\text{stat}}}{\partial \mathcal{E}_i} \right)_{A, \mathcal{E}'} = 0 \quad (45)$$

for all the internal strains. The {001} surface energies calculated using this approximation are shown in Fig. 10 as a function of temperature. The surface energy increases markedly with temperature and so it is clear that for surfaces ZSISA is a much poorer approximation than it is usually for the bulk (e.g., Ref. 15). The physical reason is that ZSISA fails to allow for the expansion between the layers in the slab as the temperature increases.

C. Li₂O

Lastly we consider briefly the temperature variation of the {111} surface of Li₂O which is a type-II surface.²⁷ The sur-

face plane consists only of Li⁺ ions with an underlying non-dipolar stacking sequence of the type



We have used the set of interatomic potentials recently derived from periodic Hartree-Fock calculations in Ref. 48. In the static limit, unrelaxed and relaxed surface energies are 0.631 and 0.582 J m⁻², respectively. These compare with a fully dynamically relaxed value of 0.601 J m⁻² at 0 K; so that, as with the {100} surface of NiO, the inclusion of vibrational terms leads to a slight increase in the surface energy. The dynamically relaxed surface energy at 300 K is 0.580 J m⁻², and 0.579 J m⁻² at 700 K, which is the smallest decrease in surface free energy with temperature of the systems examined in this paper. The onset of imaginary frequencies at the {111} surface of Li₂O, and consequent breakdown of the quasiharmonic approximation, occurs at 900 K. This is somewhat lower than the temperature (≈ 1100 K) where a superionic transition involving the Li ions is predicted for the bulk material⁴⁸ using the same set of interionic potentials.

IV. DISCUSSION

This paper has presented a method for the calculation of the fully dynamically relaxed free energies of isolated periodic slabs within the quasiharmonic approximation, based on analytic first derivatives of the free energy and second derivatives of the static energy. We have found this to be considerably more efficient for surface energies than the use of three-dimensional lattices which are constructed to produce an infinite periodic array of slabs separated by vacuum layers.⁴⁹ Detailed expressions for the lattice sums required for Coulombic interactions are given. We show how the complete set of analytic free-energy derivatives can be used for structural optimization, following which it is straightforward to generate accurately equilibrium quantities such as entropy, free energy, and heat capacity. The major part of the computational effort is usually expended in the optimization problem of the determination of the equilibrium geometry, after which calculation of the required properties is generally rapid.

For the {100} surface of NiO our temperature dependence of the surface energy is markedly smaller than that reported previously by Mulheran,²⁴ based on a crude approximation to the phonon spectrum. It is a matter of speculation as to whether larger differences would be obtained for more complicated surfaces involving more extensive structural relaxations. The close agreement between our results for NiO {100} in the static limit and those obtained from first-principles Hartree-Fock calculations⁴⁵ confirms our choice of interatomic potentials for this study, with further support for

both from surface relaxations which are within the upper bounds that have been deduced from LEED measurements.⁴⁷ Perhaps more significantly, our results highlight the inadequacy of the ZSISA approximation for surfaces. For NiO {100}, the ZSISA predicts a rapid increase in the surface energy with temperature, which is at variance with both the predictions from full dynamic relaxation and experiment.⁵⁰ While the main body of results is for simple surfaces which show relatively minor structural relaxation, the calculations for faceted {110} surfaces of MgO demonstrate that our approach is entirely suitable for much more complex surfaces, including those that are heavily defective. Finally, an important aspect of our approach is that since it is based on an exact calculation of the harmonic frequencies for all the necessary \mathbf{q} points to obtain convergence, it automatically signals the temperature at which the harmonic approximation breaks down, i.e., the onset of imaginary frequencies, thereby defining quite unambiguously the temperature regime within which meaningful comparisons with experiment might be made.

V. CONCLUSIONS

The principal conclusion of this study is that the method described by Taylor *et al.*¹⁹ for calculating the free energy of three-dimensional ionic systems based on full dynamical relaxation of the lattice structure can be applied to isolated slabs, which, if sufficiently thick, yields the full dynamical free energy and equilibrium structure of the free surface. Calculations for two faceted {110} surfaces of MgO suggest that the method could be applied to much more complex surfaces than those reported in this study.

ACKNOWLEDGMENTS

This work was supported by EPSRC Grant No. GR L31340 and the UK Facility for Computational Chemistry. G.D.B.'s contribution to this work was made possible by means of a grant from el Consejo Nacional de Investigaciones Científicas y Técnicas de la República Argentina. C.E.S. acknowledges support from EPSRC and ICI. Helpful discussions with Hugh Barron over a long period are also gratefully acknowledged.

*Also at Universidad de Buenos Aires, Facultad de Ciencias Exactas y Naturales, Departamento de Química Inorgánica, Analítica y Química Física, Pabellón 2, Ciudad Universitaria, 1428 Buenos Aires, Argentina.

¹V. E. Henrich and P. A. Cox, *The Surface Science of Metal Oxides* (Cambridge University Press, Cambridge, 1994).

²H.-J. Freund, H. Kühlenbeck, and V. Staemmler, *Rep. Prog. Phys.* **59**, 283 (1996).

³W. C. Mackrodt, *J. Chem. Soc., Faraday Trans. 2* **85**, 541 (1989).

⁴S. C. Parker, E. T. Kelsey, P. M. Oliver, and J. O. Titiloye, *Faraday Discuss.* **95**, 75 (1993).

⁵M. J. Gillan, L. N. Kantorovich, and P. J. D. Lindan, *Curr. Opin. Solid State Mater. Sci.* **1**, 820 (1996).

⁶W. C. Mackrodt, *Adv. Ceram.* **23**, 293 (1987).

⁷I. Manassidis and M. J. Gillan, *J. Am. Ceram. Soc.* **77**, 335 (1994).

⁸E. Aprá (private communication).

⁹P. Guénard, P. Renaud, A. Barbier, and M. Gautier-Soyer, in *Applications of Synchrotron Radiation to Materials Science III*, edited by L. Terminello *et al.*, MRS Symposia Proceedings No. 437 (Materials Research Society, Pittsburgh, 1996), p. 15.

¹⁰W. C. Mackrodt, R. J. Davey, S. N. Black, and R. Docherty, *J. Cryst. Growth* **80**, 441 (1987).

¹¹N. L. Allan, A. L. Rohl, D. H. Gay, C. R. A. Catlow, R. J. Davey, and W. C. Mackrodt, *Faraday Discuss.* **95**, 273 (1993).

¹²R. I. Hines, N. L. Allan, and W. R. Flavell, *J. Chem. Soc., Faraday Trans.* **92**, 2057 (1996).

¹³D. H. Gay and A. L. Rohl, *J. Chem. Soc., Faraday Trans.* **91**, 925 (1995).

¹⁴D. Fincham, W. C. Mackrodt, and P. J. Mitchell, *J. Phys.: Condens. Matter* **6**, 393 (1994).

¹⁵G. D. Barrera, M. B. Taylor, N. L. Allan, T. H. K. Barron, L. N. Kantorovich, and W. C. Mackrodt, *J. Chem. Phys.* **107**, 4337 (1997).

¹⁶M. B. Taylor, G. D. Barrera, N. L. Allan, T. H. K. Barron, and W. C. Mackrodt, *Comput. Phys. Commun.* **109**, 135 (1998).

¹⁷G. W. Watson, P. Tschaufeser, A. Wall, R. A. Jackson, and S. C. Parker, in *Computer Modelling in Inorganic Crystallography*, edited by C. R. A. Catlow (Academic, San Diego, 1997).

¹⁸N. L. Allan, T. H. K. Barron, and J. A. O. Bruno, *J. Chem. Phys.* **105**, 8300 (1996).

¹⁹M. B. Taylor, G. D. Barrera, N. L. Allan, and T. H. K. Barron, *Phys. Rev. B* **56**, 14 380 (1997).

²⁰M. B. Taylor, N. L. Allan, J. A. O. Bruno, and G. D. Barrera, *Phys. Rev. B* **59**, 353 (1999).

²¹P. W. Tasker, in *Computer Simulation of Solids*, edited by C. R. A. Catlow and W. C. Mackrodt (Springer-Verlag, Berlin, 1982), p. 288.

²²P. A. Mulheran and J. H. Harding, *Ceram. Trans.* **24**, 3 (1992).

²³P. A. Mulheran and J. H. Harding, *J. Phys. (Paris), Colloq.* **3**, C7-1971 (1993).

²⁴P. A. Mulheran, *Philos. Mag. A* **68**, 799 (1993).

²⁵D. M. Heyes, M. Barber, and J. H. R. Clarke, *J. Chem. Soc., Faraday Trans. 2* **73**, 1485 (1977).

²⁶P. M. Oliver, G. W. Watson, and S. C. Parker, *Phys. Rev. B* **52**, 5323 (1995).

²⁷P. W. Tasker, *Philos. Mag. A* **39**, 119 (1979).

²⁸G. W. Watson, E. T. Kelsey, N. H. de Leeuw, D. J. Harris, and S. C. Parker, *J. Chem. Soc., Faraday Trans.* **92**, 433 (1996).

²⁹B. G. Dick and A. W. Overhauser, *Phys. Rev.* **112**, 90 (1958).

³⁰Compare the similar Eq. (T1) of Ref. 19, where Greek superscripts were Cartesian indices 1...3; In the bulk case the orientation of the Cartesian axes is arbitrary.

³¹S. L. Cunningham, *Phys. Rev. B* **10**, 4988 (1974).

³²D. C. Wallace, *Thermodynamics of Crystals* (Wiley, New York, 1972).

³³P. J. Harley, in *Numerical Algorithms*, edited by J. L. Mohamed and J. E. Walsh (Clarendon, Oxford, 1986), p. 239.

³⁴W. H. Press, S. A. Teukolsky, W. T. Vetterling, and B. P. Flannery, *Numerical Recipes in Fortran*, 2nd ed. (Cambridge University Press, Cambridge, 1992), p. 420.

³⁵D. E. Parry, *Surf. Sci.* **49**, 433 (1975).

³⁶D. M. Heyes, M. Barber, and J. H. R. Clarke, *J. Chem. Soc., Faraday Trans. 2* **73**, 1485 (1977).

³⁷S. W. de Leeuw and J. W. Perram, *Mol. Phys.* **37**, 1313 (1979).

³⁸A. M. Stoneham and M. J. L. Sangster, *Philos. Mag. B* **52**, 717 (1985).

³⁹G. D. Barrera (private communication).

- ⁴⁰K. H. Rieder, *Surf. Sci.* **26**, 637 (1971).
- ⁴¹T. S. Chen and F. W. de Wette, *Surf. Sci.* **74**, 373 (1978).
- ⁴²T. H. K. Barron, *Thermal Expansion of Solids*, edited by R. E. Taylor, CINDAS Data Series on Materials, Vol. 1–4 (ASM International, Metals Park, OH, 1998), Chap. 1.
- ⁴³V. E. Henrich, *Surf. Sci.* **57**, 385 (1976).
- ⁴⁴A. M. Stoneham and M. J. L. Sangster, *Philos. Mag. B* **43**, 597 (1981).
- ⁴⁵J. V. Mitchell, B.Sc. thesis, University of St. Andrews, 1995.
- ⁴⁶G. C. Benson and K. S. Yun, *The Solid-Gas Interface*, edited by E. A. Flood (Arnold, London, 1967).
- ⁴⁷M. R. Welton-Cook and M. Prutton, *J. Phys. C* **13**, 3993 (1980).
- ⁴⁸R. M. Fracchia, G. D. Barrera, N. L. Allan, T. H. K. Barron, and W. C. Mackrodt, *J. Phys. Chem. Solids* **59**, 435 (1998).
- ⁴⁹C. E. Sims, Ph.D. thesis, University of Bristol, 1999.
- ⁵⁰W. D. Kingery, H. K. Bowen, and D. R. Uhlmann, *Introduction to Ceramics* (Wiley, New York, 1976).